Inflight Calibration Technique for Onboard High-Gain Antenna Pointing

Hiroshi Ohtakay*
Jet Propulsion Laboratory, Pasadena, Calif.

and

Jerome M. Hardman†
Boeing Aerospace Company, Kent, Wash.

The X-band radio frequency communication system was used for the first time in deep space planetary exploration by the Mariner 10 Venus and Mercury flyby mission. This paper presents the technique utilized for and the results of inflight calibration of high-gain antenna (HGA) pointing. Also discussed is pointing accuracy to maintain a high data transmission rate throughout the mission, including the performance of HGA pointing during the critical period of Mercury encounter.

Introduction

THE amount of information retrieved from spacecraft traveling in deep space has increased[1] by four orders of magnitude in the last decade. This great increase has been required to enable closeup observations of target planets for advanced science exploration, video data acquisition for accurate spacecraft navigation, and highly sophisticated spacecraft operation. To allow a wider bandwidth in the two-way communication system between spacecraft and ground stations for mission operations, an X-band ratio frequency communication system will play the major role in future unmanned missions.[2]

The anticipated antenna pointing performance margin required for the X-band communication system for such a mission is 0.5 dB. To meet this margin, the required high-gain antenna (HGA) pointing accuracy (Fig. 1) is 0.12° for the 1977 Mariner Jupiter/Saturn mission, and 0.14° for the 1984 Venus Orbiter mission. Such severe HGA pointing angular tolerances can be met only by accurate inflight calibration of the onboard HGA pointing system and updated error compensation.

The anticipated antenna pointing performance margin required for the X-band communication system for such a mission of 0.5 dB. To meet this margin, the required high-gain antenna (HGA) pointing accuracy (Fig. 1) is 0.12° for the 1977 Mariner Jupiter/Saturn mission, and 0.14° for the 1984 Venus Orbiter mission. Such severe HGA pointing angular tolerances can be met only by accurate inflight calibration of the onboard HGA pointing system and updated error compensation.

The Mariner 10 spacecraft was equipped with an X-band radio frequency (8.415 GHz) communication system for the first time in deep space planetary exploration. It was used for range measurement, and offered a good opportunity to demonstrate the feasibility of inflight calibration and correction of beam direction radiated from the onboard HGA.

The two basic reasons for performing inflight calibration were 1) it provided a means to recover maximum information from a spacecraft traveling in deep space, and 2) it was a prerequisite for scientific exploration of planetary atmospheres (e.g., Venus) through X- and S-band (2.295 GHz) dual-frequency occultation experiments.[3]

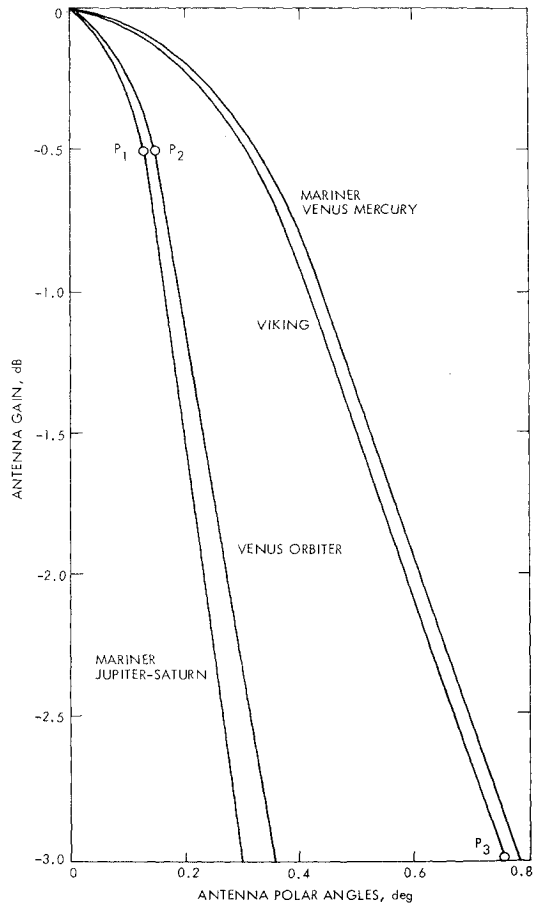

Fig. 1 HGA radiation patterns (main lobes) and system performance margin (P_1, P_2, and P_3).

Received December 4, 1974; revision received July 9, 1975. This paper presents the results of one phase of research carried out at the Jet Propulsion Laboratory, California Institute of Technology, under Contract No. NAS7-100, sponsored by the National Aeronautics and Space Administration. The authors wish to acknowledge the technical advice given by W. G. Breckenridge and V. L. Evenchuck of the Jet Propulsion Laboratory. They also would like to extend appreciation to W. I. Purdy, Jr., and W. F. Havens of the Jet Propulsion Laboratory and M. J. Flakus of the Boeing Company for data related to the inflight calibration operations.

Index categories: Spacecraft Communication Systems; Lunar and Interplanetary Spacecraft Systems, Unmanned.

*Member of Technical Staff, Guidance and Control Division.

†Guidance and Control Engineer, MVM'73 Mission Support Group.

Inflight calibration of the HGA pointing was achieved by statistically estimating mechanical, electronic, and electromagnetic errors arising in onboard sensors, antenna structures, and antenna radiation patterns during the flight.

The difficulties associated with performing inflight calibration of the HGA to enhance pointing accuracy are the facts that 1) the spacecraft is subject to attitude limit cycle motion that, for the Mariner 10, amounted to $\pm 0.25°$ about the spacecraft pitch, yaw, and roll axes, whereas the radiation pattern of the onboard HGA for the X-band ratio frequency was extremely narrow (Fig. 1); 2) signal strength measurements of the X-band radio signal at ground stations are disturbed by continuously changing atmospheric conditions of the Earth; 3) mechanical alignment of the HGA Articulation and Pointing Subsystem (APS) could have different characteristics from those measured on Earth prior to launch because of mechanical shock during launch and deployment in a zero gravity environment of the 2-m boom which the antenna is mounted; and 4) the continuously changing configuration of sunlight and spacecraft orientation causes slowly varying thermal distortion of the HGA and actuator structures.

To overcome these difficulties, a mathematical model that included mechanical, electronic, and electromagnetic error parameters associated with the HGA pointing system was developed. A weighted minimum-variance estimation algorithm[4] was utilized to statistically estimate the error parameters based on signal strength measurements of X-band radio signals and engineering telemetry values, both taken during inflight calibration.

The inflight calibration schedule of the HGA during the Mariner 10 mission was carefully planned through computer simultation prior to the mission so that the inflight calibrations could cover the maximum range of actuator angles that vary according to spacecraft trajectory. Four inflight calibrations before the Venus encounter on February 5th, 1974, were performed; they resulted in a calibration accuracy represented by a one-sigma error ellipse with semimajor and semiminor axes being 1.6 and 0.9 arc-min in the antenna coordinate system. Five calibrations during the flight of the spacecraft between Venus and Mercury enhanced the calibration accuracy, represented by an error ellipse of 0.7 and 0.6 arc-min for its semimajor and semiminor axes.

Communication Systems and Spacecraft Description

Mariner 10's onboard HGA consisted of a paraboloidal reflector with a 1.37-m diam circular aperture and radiating feeds for S- and X-band operation. The radiated electromagnetic wave from this antenna was right-hand circularly polarized. After the Mariner 10 launch, the HGA boom was deployed to a predetermined nominal position, which allowed the HGA to point in all directions (except those obscured by the spacecraft) by controlling two independent gimbaled actuators. The first (boom) actuator was mounted at the tip of the antenna boom. The second (dish) actuator was mounted perpendicular to the boom actuator; the antenna dish was mounted such that the antenna boresight was perpendicular to the dish actuator.

The spacecraft attitude reference was provided by celestial sensors except during the Sun occultation period, during which the spacecraft attitude was referenced to onboard inertial instruments. The celestial sensors for attitude reference include a pair of Sun sensors, whose null planes were mutually orthogonal, and a star tracker mounted with its light-sensitive axis perpendicular to the intersection of the null planes of the Sun sensors. Error signals detected by the attitude reference sensors were input to switching amplifiers that activated attitude control gas jets when the error signals exceeded a specified threshold value ($\pm 0.25°$). The attitude position errors were also supplied to the onboard S-band modulator for transmission to the Deep Space Network (DSN) station.

Antenna Gain Function

Knowledge of the Mariner 10 antenna radiation pattern (measured prior to launch) provided the essential clue to knowing the radiation pattern of the HGA during flight. Systematic observations of signal strength measurements during flight revealed the relative configuration of the radiating and receiving antennas. To facilitate a closed-loop solution fo the calibration problem, an analytic model of the HGA gain function was essential. The antenna gain function G is generally a complicated relationship that depends upon the type of antenna, the type of feed, the structure on which the antenna and the feed are mounted, and the perturbation due to fabrication errors.[5] An accurate, simple mathematical model around the peak of the main lobe was developed for the purpose of the inflight calibration since calibration measurements had been planned to be taken only in the range of the antenna cone angles that provided from 0 dB to about -10 dB in the signal strength measurements

$$G(\theta) = k_1 \left[\frac{\sin k_2 \theta}{\theta} \right]^2 \tag{1}$$

where k_1 = gain constant, k_2 = beam width constant, and θ = angle off axis (in radians).

The change of signal strength measurements of radio signals transmitted by an antenna whose boresight vector lay off by the angle θ from that of a receiving antenna is given by

$$S(\theta) = 10 \log_{10} G(\theta) \tag{2}$$

The feasibility of this mathematical model was examined against the measured radiation pattern of the onboard HGA prior to spacecraft launch. Discrepancies between the mathematical model and the measured radiation pattern of the main lobe were confirmed to be less than 0.1 dBm (1σ) and were treated as a part of the measurement noise explained in the next section.

Error Sources and Models

Two types of error sources should be considered in determining the HGA pointing accuracy when it is commanded to point in an arbitrary direction: control type and knowledge type. Control-type error sources, which cannot be reduced by calibration, include limit cycle motion of the spacecraft, and APS command and execution resolution. Knowledge-type error sources include antenna structural offset errors, onboard sensor offset and scale factors, and unknown

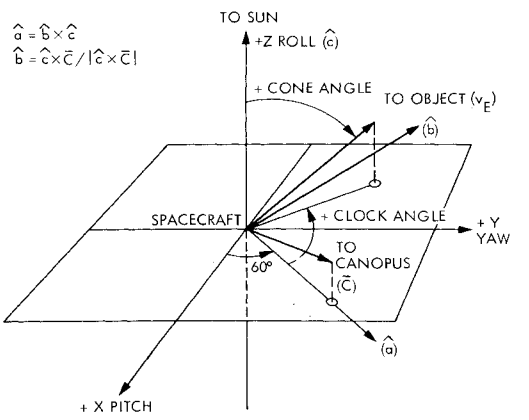

Fig. 2 Spacecraft body fixed celestial coordinate system and object direction. Cone angle of object: the angle from the spacecraft + roll axis to the spacecraft/object vector. Clock angle of object: the angle measured clockwise (when looking in the + roll direction) from the spacecraft roll axis/Canopus tracker plane to the spacecraft roll axis/object plane.

parameters associated with the HGA radiation pattern. Once these fixed error sources and characteristics are identified, the errors can be calibrated and the antenna pointing accuracy enhanced. Knowledge-type errors also include random errors, e.g., sensor noise and telemetry resolution. The fixed knowledge-type errors also affect control accuracy. In the following material, the knowledge-type fixed error sources are identified and characterized through mathematical models.

Spacecraft navigation based upon spacecraft range and range-rate measurements provides information about spacecraft position in the celestially-fixed inertial frame. This information is incorporated into a spacecraft-Earth vector (Fig. 2)

$$\hat{v}_E = \text{col}(\sin\beta\cos\alpha, \sin\beta\sin\alpha, \cos\beta) \tag{3}$$

where α, β = clock and cone angles, respectively, and col ( ) = column vector.

To determine the spacecraft-Earth vector relative to the antenna boresight direction, $\hat{v}_E$ must be expressed in the antenna coordinate system. This is accomplished through successive transformations of $\hat{v}_E$ into various spacecraft-structure-fixed coordinate systems, summarized in Table 1.

The true coordinate systems, in general, differ from the nominal systems because of errors caused by spacecraft-navigation residuals, errors arising in onboard sensor electronics and telemetry channels, and mechanical misalignments introduced during spacecraft fabirication as well as those caused by gravitational and thermal environmental changes, and deformation of the radiation pattern of the HGA. The composite effects of these errors may be completely represented by a skew-symmetric matrix:

$$E = \begin{bmatrix} 0 & \epsilon_3 & -\epsilon_2 \\ -\epsilon_3 & 0 & \epsilon_1 \\ \epsilon_2 & -\epsilon_1 & 0 \end{bmatrix} \tag{4}$$

provided ϵ's are small. Furthermore, definition of a cross product operator $\otimes$ for a vector v such that $\epsilon \otimes v = -E\,v$ where $\epsilon = \text{col}\ (\epsilon_1, \epsilon_2, \epsilon_3)$ suffices to fine error vectors e's associated with each coordinate transformation, since it holds that

$$\epsilon = \sum_{i=1}^{5} T_{1i} e_i \tag{5}$$

where T's are defined in Table 1. In this equation, ϵ_1, ϵ_2, and ϵ_3 represent cumulative errors in dish, cross-dish (defined as perpendicular to the dish direction), and rotation directions. The single θ between antenna boresight and the Earth vector is now given by

$$\theta = \cos^{-1}(\hat{\xi}\cdot\hat{\zeta}) \tag{6}$$

where $\hat{\zeta}$ is the antenna boresight unit vector, and

$$\xi = (I+E)\,T_{15}\hat{v}_E$$

Since $\hat{\zeta}$ is a known quantity, the rest of this section is devoted to identifying error sources that constitute the error vector ϵ.

The spacecraft body-fixed $a'b'c'$ coordinate system deviates from the celestially fixed abc coordinate system because of spacecraft attitude control limit cycles about the celestial references. The pitch, yaw, and roll attitude sensor telemetry signals, denoted by θ_p, θ_y, and θ_r, respectively, differ from the true values, marked by an asterisk, as

$$\theta_q = \delta\theta_{q0} + (1+\delta K_q)\,\theta_q^* \tag{7}$$

where $q \in \{p, y, r\}$, $\delta\theta_{q0}$ = null offset, and δK_q = scale factor error.

The sensor null offsets are caused by sensor mounting errors and bias drift in switching amplifier electronics, while

Table 1 Spacecraft structure fixed coordinate systems

Description: designation	Definition[a]	Transformation matrix[b]
Celestially fixed *abc*: A	$\hat{a}=\hat{b}\times\hat{c}\ \hat{b}=\hat{c}\times\hat{C}/\lvert\hat{c}\times\hat{C}\rvert$ $\hat{c}$ = Sun unit vector, $\hat{C}$ = Star unit vector	
Spacecraft XYZ before attitude control rotation: X	Rot $(\alpha_x,3)$ from A	T_{56}
Spacecraft XYZ after attitude control rotation: X'	Rot $(\phi_r,3)$ Rot $(\phi_y,2)$ Rot $(\phi_p,1)$	
Spacecraft body fixed $a'a'c': A'$	Rot$^{-1}(\alpha_x,3)$from X'	
HGA zero reference after clock angle setting: K	Rot $(\alpha_B,3)$ from A′	T_{45}
HGA zero reference after cone angle setting: N	Rot$(-\pi/2+\beta_B,2)$ from K	T_{34}
HGA rotating after boom angle setting: B	Rot $(\psi_B,1)$ from N	T_{23}
HGA rotating after dish angle setting: D	Rot $(\psi_D,2)$from B	T_{23}
HGA coordinate: G	Nominally identical with D	T_{11}

[a] Rot (α, I) defines a positive rotation around the Ith axis by the angle of α. [b] $T_{ij} = T_{ik}T_{kj}$ and T_{11} = an identity matrix.

the scale factor errors is the deviation of sensor scale factor from ground calibrated values. The set of sensor angles and the attitude (pitch, yaw, roll) angles ϕ are to the first order

$$\phi_q = \theta_q + K(r, q)\,[\cos\alpha_x \cot\beta_s \theta_t - \sin\alpha_x \cot\beta_s \theta_y] \tag{8}$$

where β_s = cone angle of reference star (Canopus), α_x = spacecraft structure constant, and

$$K(r,q) = \begin{cases} 1: & q=r \\ 0: & \text{otherwise} \end{cases}$$

Hence, the sensor and attitude angle errors, i.e., $\delta\phi$, also maintain a relationship of the same form. Attitude sensor-related error paremeters are given by

$$e_5 = \text{col}(\delta\phi_p, \delta\phi_y, \delta\phi_r) \tag{9}$$

The true deployment configuration would deviate slightly from what had been planned in the Mariner 10 mission because of fabrication error, the deployment in zero gravity environment, and the thermal effects. The deviations would be represented by

$$e_4 = \text{col}(0, 0, \delta\alpha_B) \tag{10a}$$

$$e_3 = \text{col}(0, \delta\beta_B, 0) \tag{10b}$$

Two mutually-independent error sources associated with the boom actuator are considered. One is nonorthogonality, $\delta\phi_{12}$, between the boom and the dish actuator axes, which results from fabrication error and mechanical misalignment during deployment. The other is a discrepancy, $\delta\psi_{B0} + \delta\psi_{B1}$, between the telemetered boom angle and its true value, where $\delta\psi_{B0}$ is attributed to boom potentiometer null offset, and $\delta\psi_{B1}$ is due to actuator mechanical backlash and telemetry data quantization and resolution error:

$$e_2 = \text{col}(\delta\psi_{B0} + \delta\psi_{B1}, 0, \delta\phi_{12}) \tag{11}$$

It should be noted that a value of $\delta\psi_{B1}$ could change whenever the boom actuator is commanded to be slewed, whereas a value of $\delta\psi_{B0}$ stayed constant.

In defining the true antenna coordinate system, the three independent error sources are the following: 1) a small twist error of the antenna frame, caused by mechanical as well as electromagnetic asymmetry around the boresight, is modeled by a small angle δR rotation about the first axis; 2) the second and third axes may be nonorthogonal, $\delta\phi_{23}$; 3) the telemetered dish angle value, i.e., ψ_D, deviates from its true value by $\delta\psi_{D0} + \delta\psi_{D1}$, where $\delta\psi_{D0}$ denotes the dish actuator potentiometer null offset and $\delta\psi_{D1}$ represents backlash and quantization error. The error $\delta\psi_{D1}$ remains constant if successive telemetry values do not change; otherwise, $\delta\psi_{D1}$ changes its value, whereas $\delta\psi_{D0}$ stays constant. Thus, the error vector e_1 is given by

$$e_1 = \text{col}(\delta\phi_{23}, \delta\psi_{D0} + \delta\psi_{D1}, \delta R) \tag{12}$$

It should be noted that values of δR, $\delta\phi_{23}$, and possibly $\delta\psi_{D0}$ for X-band carrier signals differ from those for S-band.

During the Mariner 10 HGA inflight calibration, navigation residual error typically ranged about 100 km (1σ), resulting in at most a 0.5 arc-sec (1σ) deviation in the celestially-fixed inertial frame. It was concluded that this caused an insignificant contribution to the HGA pointing composite error.

The ground station automatic gain control (AGC) generates voltages proportional to a 5-sec average of the signal strength of S- and X-band carrier frequencies. Error sources arising at the ground stations are mostly electronic and electromagnetic. Constant offset-type error sources include DC bias drift in AGC electronics, bias error in signal strength measurements due to time averaging, and the bias constant k_1 in Eq. (1).

The random noise power components added to the signal strength measurements are contributed by two sources: one is inherent to the antenna environment; the other is indirectly introduced from engineering telemetry channel noise and the onboard antenna modeling residual errors. The antenna-originated noise is generally known in terms of noise temperature and is due to electromagnetic radiation generated by celestial bodies within the antenna beam, atmospheric absorption and reradiation, and by physical bodies surrounding the antenna. The weather-induced noise temperature of the DSN antennas[6] when aimed at a cold sky (i.e., there are no major celestial sources around the antenna boresight) is given by

$$T(\gamma) = C_1 + \Delta T(\gamma) + C_2/\sin\gamma \tag{13}$$

where C_1, C_2 = noise temperature constants, ΔT = noise temperature on a clear day, and γ = DSN antenna elevation angle.

The predicted antenna noise temperature for the period November 1973-March 1974 based upon the past observation data was 35.0 K (3σ) or, equivalently, 0.14 dB (1σ). Random noise, assumed to be normally distributed, in attitude telemetry channels and gimbaled actuator angle telemetry channels was mapped onto signal strength measurements through the relations described in Eqs. (1-6). The onboard HGA modeling residual errors, measured to be less than 0.1 dBm at prelaunch calibration, were also added to the random noise in the signal strength measurement model.

Inflight Calibration Strategy and Algorithm

The nominal gimbaled actuator angles for the desired antenna directional pointing can be obtained by solving for boom (ψ_B) and dish (ψ_D) in the error free system

$$\hat{\zeta} = T_{15}\hat{v}_E \tag{14}$$

The solution pair (ψ_B, ψ_D) is time-varying since $\hat{v}_E$ is a time-varying vector function determined by the spacecraft trajectory with no respect to the Earth. A maximum of two sets of solutions (primary and secondary) are possibly subject to constraints (Fig. 3) imposed by the electrical and mechanical configuration of the APS. The error parameters and the HGA radiation pattern parameters could take values different from those measured prior to spacecraft flight; therefore, the inflight calibration of the HGA pointing is a statistical estimation of the time-invarient parameter set

$$x = \text{col}(\delta\phi_{23}, \delta\psi_{D0}, \delta\phi_{12}, \delta\psi_{B0}, \delta\beta_B, \delta\theta_{p0}, \delta\theta_{y0}, \delta\theta_{r0}, k_1, k_2) \tag{15}$$

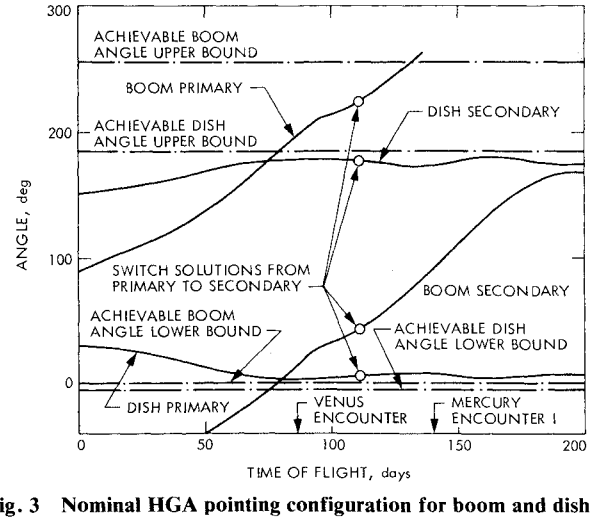

Fig. 3 Nominal HGA pointing configuration for boom and dish actuators.

Prelaunch calibration simulation justified the reduction of the original parameter set to this ten parameter set with relatively little effect on the signal strength measurement. The error paremeters $\delta\psi_{DI}$ and $\delta\psi_{BI}$, which characterized the backlash of the gimbal system, were solved for separately after the estimate of the paremeters in Eq. (15) had reached sufficient convergence.

To obtain good statistical estimates of the individual parameter values in addition to the antenna boresight direction, it is required that a sufficient number (I), i.e., greater than 10, of signal strength measurements for the different actuator angle configurations be taken. It is also required that the antenna movement be restricted to the main lobe where the mathematical model utilized represents the true radiation pattern. These conditions are satisfied by using a backlash independent slew pattern described in Fig. 4, with an adequate time period at each stationary point for collecting transient free signal strength measurement data. The inflight calibration is based upon a set of signal strength measurement data that is taken consistently on the positive side of the backlash hysteresis: measurement points 1, 2, 3, 5, 7, 8, and 9 of Fig. 4. This approach makes it possible to determine the magnitude of the backlash in each axis by comparing the signal strength measurement data taken on the one side of the backlash hysteresis. A weighted minimum variance estimation algorithm is iterately applied to estimate the individual paremeter values as well as the resulting calibration accuracy in the antenna pointing.

The most comprehensive measure for HGA inflight calibration performance would be the resulting accuracy of the onboard HGA pointing in any desired direction. This quantity is defined by a 3×3 covariance matrix

$$A_{cc} = F P_K(I) F^T \tag{16}$$

with F being a 3×10 matrix defined as

$$F = \partial\epsilon / \partial x \tag{17}$$

evaluated at the latest values of the set of error parameters defined in Eq. (15) and at any desired angles of boom and dish actuators, and $P_K(I)$ being the a posteriori covariance matrix at the K-th inflight calibration. In particular, A_{cc} evaluated with F corresponding to the most updated values of boom and dish actuators to point to the Earth immediately after inflight calibration was selected to be used as the inflight calibration performance index.

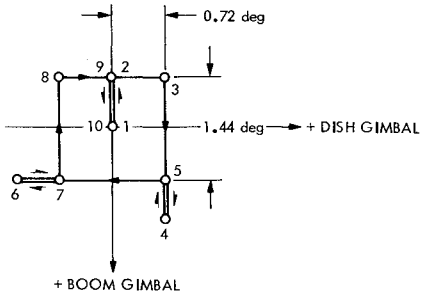

Fig. 4 HGA slew dither pattern.

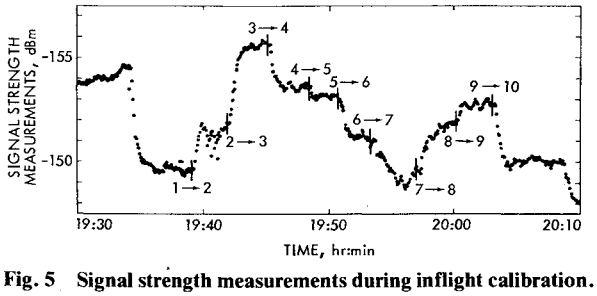

Fig. 5 Signal strength measurements during inflight calibration.

Inflight Calibration Results

The inflight HGA calibration schedule was planned on the basis of computer simulations conducted prior to launch. The basic planning philosphy was as follows: first, inflight calibrations were to be distributed evenly so that the greatest range of actuator angles could be covered to produce a uniform HGA pointing accuracy; second, calibrations were to be conducted without interference with other mission activities having priority. Also, at least one calibration was to be performed close to each of the critical periods of the mission, i.e., encounter with the target planets.

Four HGA calibrations were performed during flight prior to the encounter with Venus. Five inflight calibrations were made during the Venus-to-Mercury flight leg before the first Mercury encounter. Typical signal strength measurements for one inflight calibration, which took about 40 minutes, are shown in Fig. 5. Sharp rises and falls in the signal strength measurements represent transient responses to commanded slews. A time delay before and an overshoot after a transient response in signal strength measurements, both lasting for 5-10 sec, were observed. The former was apparently caused by a composite effect of signal lag in AGC electronics and time averaging of signal strength measurements, and the latter by under-damped characteristics of AGC electronics. To avoid false measurements, signal strength data immediately before and after a transient had been removed from further processing. Signal strength measurement data and relevant HGA calibration engineering telemetry data were time tagged by both spacecraft the DSN station clocks. This facilitated synchronization of observation data from different subsystem data sources and accounted for time delay in radio signal transmission from the spacecraft.

Figure 6 shows directions and magnitudes of actuator gimbal angle corrections immediately after each inflight calibration. In this figure, the gradual decrease in magnitudes of angle corrections in the first four calibrations indicates a convergent process of HGA pointing error correction. Sudden increase in magnitudes at the sixth inflight calibration was a result of changing solution sets (flip-flop) for the HGA gimbal angles. Repeated inflight calibrations after the reorientation reidentified the new pointing error resulting in a gradual decrease in magnitudes in angular compensation. Changes in signs of correction angles were caused by possible

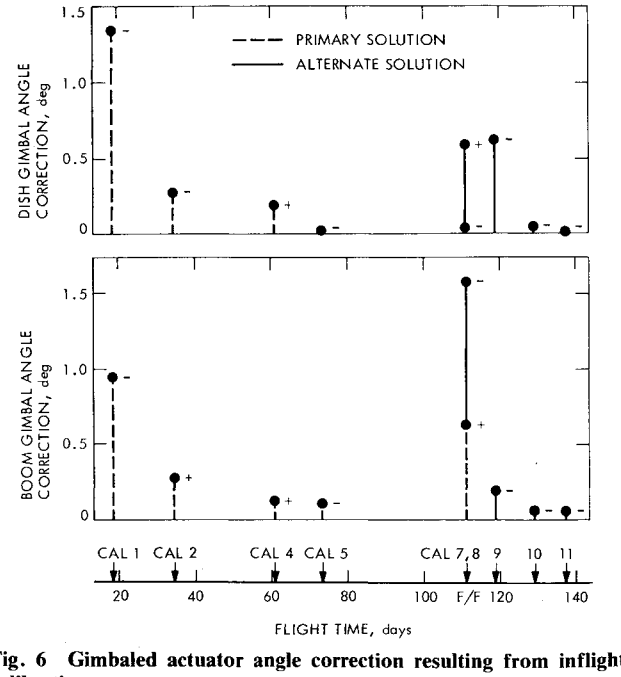

Fig. 6 Gimbaled actuator angle correction resulting from inflight calibration.

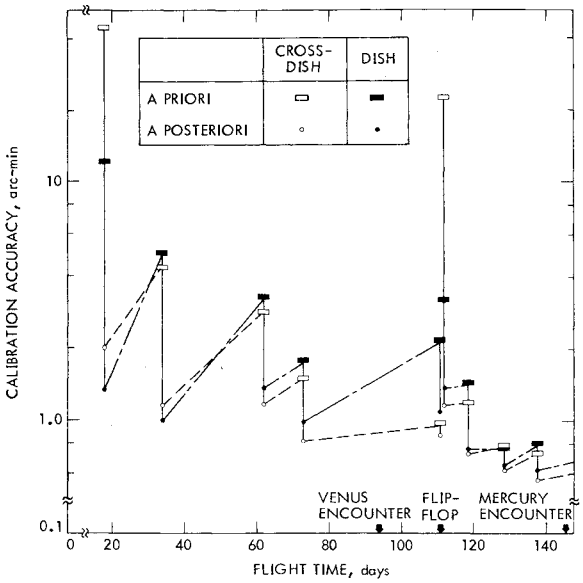

Fig. 7 Time evolution of HGA pointing calibration accuracy.

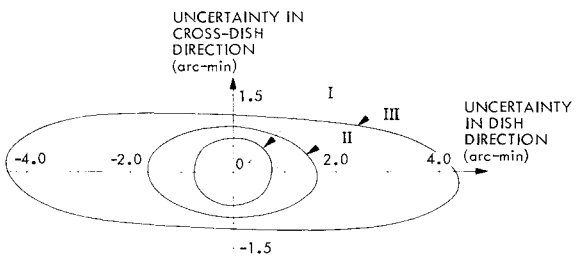

I. ONE-SIGMA ERROR ELLIPSE AT MERCURY ENCOUNTER
II. ONE-SIGMA ERROR ELLIPSE AT VENUS ENCOUNTER
III. ONE-TENTH-SIGMA ERROR ELLIPSE AT SPACECRAFT LAUNCH

Fig. 8 HGA pointing calibration error ellipses.

overcompensation in previous calibration and time varying effects of the error paremeter estimation algorithm.

The time evolution of the HGA pointing calibration accuracy is delineated in Fig. 7. In this figure, the upward slopes of the curves between two successive calibrations were caused by time-varying elements of HGA pointing accuracy evaluation functions. The length of vertical lines represents a degree of restoration of HGA pointing calibration accuracy in the dish and the cross-dish directions accomplished at each calibration.

The error ellipses associated with HGA pointing accuracy were constructed from the 2×2 partition of A_{cc} given by Eq. (6) associated with the dish and the cross-dish directions. Significant differences in HGA pointing calibration accuracies of the dish and the cross-dish directions were observed at the Venus encounter. The resulting uncertainty (Fig. 8) of HGA pointing in the dish direction was greater than that in the cross-dish direction by almost a factor of 2, while almost identical pointing accuracy in both dish and cross-dish directions was achieved at the Mercury encounter.

The separation angle between the HGA boresight direction and the spacecraft-Earth vector including both knowledge and

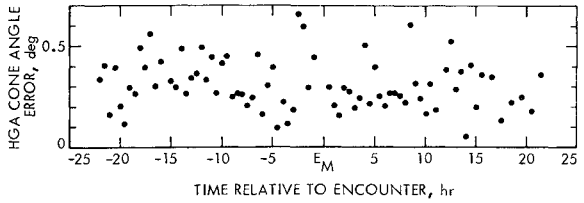

Fig. 9 HGA pointing error at Mercury encounter.

control-type errors is a measurement of the HGA pointing performance. Figure 9 illustrates such actual HGA pointing performance during the spacecraft Mercury encounter period. The largest error sources contributing to this result were found to be the spacecraft attitude limit cycle motion and changes of the optimal set of estimated error parameters due to the time-varying coefficients.

Conclusions

The feasibility of inflight calibration of onboard HGA pointing was demonstrated for the X-band radio frequency communication system used for the first time in deep space planetary exploration. The inflight calibration of HGA pointing significantly improved HGA pointing accuracy by compensating for the errors in the antenna pointing mechanism; this compensation resulted in error ellipses whose semimajor axes were less than 1.6 and 0.7 arc-min at spacecraft encounters with Venus and Mercury, respectively. A simple mathematical model of a symmetric function (around its boresight) was shown to be a sufficiently accurate representation of the onboard HGA radiation pattern for the main lobe.

The actual HGA pointing performance was found to be slightly above 0.5° during the Mercury encounter period. A significant improvement of the ultimate HGA pointing performance can be accomplished by coping with the major error sources, which is the limit cycle motion of the spacecraft. Approaches for this purpose include reduction of spacecraft limit cycle motion by narrowing the deadband width at least during critical periods of a mission, and implementation of an onboard autonomous HGA pointing mechanism designed to compensate spacecraft limit cycle motion.

References

[1] Renzetti, N.A., et al., "The Deep Space Network Progress Report for November and December 1973," Tech. Rept. 32-1526, Vol. XIX, Feb. 1974, Jet Propulsion Laboratory, Pasadena, Calif.

[2] Bourke, R.D., Miles, R.F., Penzo, P.A., Van Dillen, S.L., and Wallace, R.A., "Mariner Jupiter/Saturn 1977 Preliminary Mission Design," AIAA Paper 72-943, Palo Alto, Calif., 1972.

[3] Michael, W.H., Jr., et Al., "Radio Science Experiments," *Icarus*, Vol. 16, 1972, pp. 55-73.

[4] Sage, A.P. and Melsa, J.T., *Estimation Theory With Applications to Communications and Control*, McGraw-Hill Book Co., Inc., New York, 1971.

[5] Rush, W.V.T. and Potter, P.D., *Analysis of Reflector Antennas*, Academic Press, New York, 1970.

[6] Edelson, R.E. et al, "Telecommunications Systems Design Techniques Handbook," Tech. Memo. 33-571, July 1972, Jet Propulsion Laboratory, Pasadena, Calif.